analytical chemistry

pubs.acs.org/ac Article

Iodinated BSA Nanoparticles for Macrophage-Mediated CT Imaging and Repair of Gastritis

Yanxian Wu,[‖] Jun Gu,[‖] Shaodian Zhang, Yuan Gu, Jie Ma, Yangyun Wang,* Leshuai W. Zhang, and Yong Wang*

Cite This: https://doi.org/10.1021/acs.analchem.0c05407 Read Online

ACCESS | Metrics & More | Article Recommendations | Supporting Information

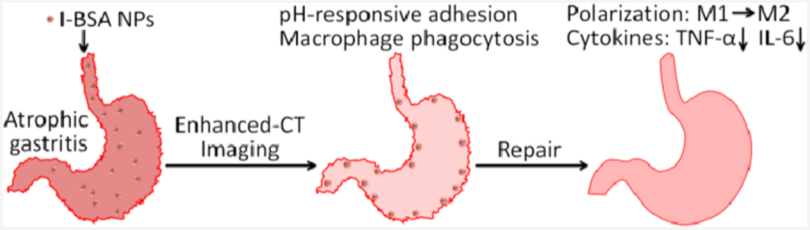

ABSTRACT: The development of a specific and noninvasive technology for understanding gastritic response together with efficient therapy is an urgent clinical issue. Herein, we fabricated a novel iodinated bovine serum albumin (BSA) nanoparticle based on gastritic microenvironment for computed tomography (CT) imaging and repair of acute gastritis. Derived from the characteristic mucosa defect and inflammatory cell (e.g., macrophage and neutrophil) infiltration in acute gastritis, the pH-sensitive nanoparticles can sedimentate under acidic conditions and be uniformly distributed in the defected mucosal via the phagocytosis of inflammatory cells. Hence, enhanced CT images can clearly reveal the mucosal morphology in the nanoparticle-treated gastritic rat over a long time window comparison with nanoparticle-treated healthy rats and clinical small-molecule-treated gastritic rat. In addition, we have discovered that nanoparticles can repair the atrophic gastric mucosa to a normal state. This repair process mainly stems from inflammatory immune response caused by phagocytized nanoparticles, such as the polarization of proinflammatory macrophages (M1) to anti-inflammatory macrophages (M2). The biocompatible nanoparticles that avoid the inherent defects of the clinical small molecules have great potential for accurate diagnosis and treatment of gastritis in the early stage.

INTRODUCTION

Gastritis often accompanies structural mucosal changes caused by various pathogenic factors such as physical, chemical, pharmaceutical, and biological.[1−4] Atrophic gastritis is a premalignant condition associated with increased cancer risk.[5] Nowadays, X-ray barium radiography and endoscope combined with biopsy are major clinical tools for gastritis diagnosis, while these methods with complicated procedures and poor patient experience are far from clinical needs.[6,7] Therefore, it is very meaningful to exploit a facile, noninvasive diagnosis platform for gastritis.

X-ray computed tomography (CT) is one of the clinically most frequently used noninvasive diagnostic tools.[8] Convenient and efficient CT should be an option for assessing potential gastric disease in patients, especially in the emergency department.[9] Clinically, exogenous CT contrast agents are indispensable for enhancing the image sensitivity of soft tissues.[10] 15 FDA-approved small-molecule iodinated contrast agents have currently been the choice for clinical CT applications.[11] However, there are several challenges to the current generation of iodinated contrast agents, such as nonspecificity, potential renal failure risk, and possible iodine hypersensitivity.[12] Especially, the imaging time window for CT following administration of the contrast agents is typically very narrow due to the low molecular weight, short blood circulation, and rapid renal clearance profiles.[13] All these shortcomings can cause missed diagnosis of the disease and poor patient experience.[14] Therefore, it is imperative to develop novel CT contrast agents to better meet clinical needs.

To date, many attempts have been made on nanosized CT contrast agents from high X-ray attenuated elements including Yb,[15] Hf,[16] Ta,[17] Au,[18] and Bi.[19,20] These inorganic nanoparticles have not yet satisfied the needs of clinic contrast due to the unclear biosafety of heavy metals.[21,22] Alternatively, some typical polymeric nanostructures have also been applied for enhanced CT from the high payloads of iodinated small molecules.[23−25] For example, Hyafil et al. pioneered an iodinated N1177 nanoemulsion for macrophage imaging in sufficient time windows.[23] Moreover, iodine was labeled on the

Received: December 24, 2020
Accepted: March 19, 2021

https://doi.org/10.1021/acs.analchem.0c05407
Anal. Chem. XXXX, XXX, XXX−XXX

tyrosine residues in albumin nanoparticles by the chloramines-T method, thereby constructing CT nanoagents.[26,27] However, once exposed to the physiological environment, the encapsulated small molecules or labeled iodine may be accidentally out of these nanostructures, which may complicate the image analysis and hinder the clinical practice.[28] For this challenge, the conjugate or cross-linking strategy should be an optimal solution derived from activatable functional groups of commercial iodinated small molecules.[29−31] Typically, a cross-linked poly(iohexol) nanoparticle has been fabricated to acquire long-term CT potentiation images without multiple administrations.[29] To further improve the specificity of enhanced CT, advanced covalent polymer nanoparticles were modified using targeting moieties to overcome the intrinsic limitation of clinic contrast.[32−35] Current progress is mainly focused on targeted cancer imaging;[36] no corresponding nanoparticles have yet been developed for inflammation. Especially in acute gastritis, the stimulation of the gastric mucosa by external factors can lead to mucosa defect and inflammation.[37] Therefore, new advances in long-circulating and microenvironment-sensitive nanoparticles may offer promise in understanding the gastritic response together with efficient therapy.[38]

Herein, we aimed to develop a novel iodinated nanoparticle with bovine serum albumin (BSA) and iohexol for CT imaging and repair of gastritis. As a clinically used small-molecule agent, iohexol can be oxidized to iohexaldehyde. This highly oxidized molecule is used as a cross-linking agent to induce the assembly of BSA molecules via the aldimine condensation reaction. Different from the deiodination defects of the nanoparticles prepared earlier, the nanoparticles have better stability. The prepared iodinated BSA nanoparticles (I-BSA NPs) can adhere to the mucosa surface of gastritis resulting from pH-responsive sedimentation. The infiltrating inflammatory cells will subsequently phagocytize the sedimentary I-BSA NPs, so the appearance and severity of gastritis can be uniformly visible by I-BSA NPs enhanced CT imaging over a long time window. Interestingly, the I-BSA NPs also have a good repair function for acute gastritis via the polarization of proinflammatory macrophages (M1) to anti-inflammatory macrophages (M2). The biocompatible nanoparticles have potential applications in long-term window imaging and treatment of gastritis.

MATERIALS AND METHODS

Synthesis of Iohexaldehyde. In brief, 1.64 g (2 mmol) of iohexol was dissolved in 10 mL water and cooled to 0 °C. An excess amount of $NaIO_4$ (10 mmol, 1.67 equiv per 1,2-diol group) dissolved in 6 mL of water was added dropwise into the above iohexol aqueous under nitrogen with magnetic stirring. The reaction mixture was allowed to precede 2 h under nitrogen at 0 °C in the dark. After filtration, evaporation, and recrystallization in methanol, the yellowish powder iohexaldehyde was obtained with a yield of over 60%.

Preparation of I-BSA NPs. In a 20 mL volumetric flask, 2 mL of absolute ethyl alcohol was added dropwise into 1 mL of BSA solution (10 mg mL^{-1}) under vigorous stirring at 25 °C. After 10 min, 1 mL of iohexaldehyde solution (17 mg mL^{-1}) was added dropwise into the above mixture and continued to react for 48 h at 25 °C. With the addition of iohexaldehyde, the pale blue solution gradually turned to a transparent solution of golden yellow. After the reaction, the final solution was centrifuged (8000 rpm, 15 min), then colloidal supernatant was filtrated with 10 kDa membrane and washed with water several times to remove absolute ethyl alcohol and other impurities, and finally condensed to 0.5 mL. The final sample was stored at 4 °C for later use.

In Vitro X-ray Attenuation Coefficient. The contrast efficacy of I-BSA NPs was first compared with iohexol. I-BSA NPs and iohexol was diluted into a series of equal concentrations of iodine with deionized water. Deionized water was used as a control. All of the samples were scanned on a SPECT/CT system (MILABS, Netherlands).

In Vivo CT Imaging. For acute gastritis CT imaging, nine Sprague−Dawley (SD) rats were randomly split into three groups: I-BSA NP-treated normal rats, I-BSA NP-treated model rats, and iohexol-treated model rats (n = 3). The rats were given 1 mL of I-BSA NPs or iohexol (iodine concentration was 10 mg mL^{-1}) intragastrically 4 h after the model was established, and the CT images were scanned using a U-SPECT/CT system (MILABS, Netherlands) at certain intervals. The parameter setting was the same as above.

Immunofluorescence Analysis. To clarify whether I-BSA NPs accumulate in inflammatory cells, the healthy and modeled rats were administered intragastrically with the cypate-labeled I-BSA NPs. At 24 h after the administration of I-BSA NPs, the entire rat stomach was sectioned and immunostained. Briefly, sectioned stomachs were washed with phosphate-buffered saline (PBS) (0.1 mol L^{-1}, pH 7.4) for 10 min. Sections were blocked using PBS with 5% (v/v) BSA for 1 h, followed by incubating samples with primary antibodies in blocking solution overnight at 4 °C. Then, the sections were washed three times with PBS (0.1 mol L^{-1}, pH 7.4) and incubated with fluorophore-marked secondary antibodies for 1 h at 25 °C. The samples were washed again and incubated in 4′,6-diamidino-2-phenylindole (DAPI) for 10 min. Finally, images of the specimens were acquired using a confocal microscope (FV1200, Olympus).

Immunohistochemistry Analysis. To observe the macrophage phenotype, the rats were split into three groups: normal group, untreated gastritis group, and I-BSA NP-treated gastritis group. After treating for 24 h, the gastritis tissues of all three groups were collected for immunohistochemical staining of CD206. The specific immunohistochemical staining steps are as follows. First, paraffin sections were dewaxed and sealed with 3% BSA at 25 °C for 30 min and then incubated with primary antibody overnight at 4 °C. After washing with PBS three times, the second antibody was added and incubated at 25 °C for 50 min. Then, 3,3′-diaminobenzidine (DAB) was added for coloration. The positive was brown yellow. Finally, the nuclei were stained with hematoxylin before the samples were dehydrated and mounted. The samples were observed under a microscope (IX73, Olympus) at 200× magnification.

RESULTS AND DISCUSSION

Our strategy is to fabricate a biocompatible and microenvironment-sensitive nanoparticle for CT imaging and repair of acute gastritis based on the clinical small-molecule contrast agents. We herein choose iohexol and BSA to prepare the objective nanoparticles, namely, I-BSA NPs. To synthesize I-BSA NPs, as shown in Figure S1A, iohexol was first oxidized to iohexaldehyde with periodic acid under certain conditions. The oxidation products were characterized by ^1H NMR shown in Figure S1B. Peak (a) with 8.46 ppm corresponds to aldehyde protons, while peaks (b) at about 2.50 ppm are assigned to the methylene protons connected to the aldehyde

https://doi.org/10.1021/acs.analchem.0c05407
Anal. Chem. XXXX, XXX, XXX−XXX

groups, and methyl proton peak (c) of the acetyl group appears at 1.63 ppm. The relative integration ratio of the peaks (b) to the peak (c) in the ^{1}H NMR spectra is 2:1, which is close to the theoretical ratio between methylene protons and methyl protons. All these results indicate a successful synthesis of iohexaldehyde. The design strategy given in Figure 1A

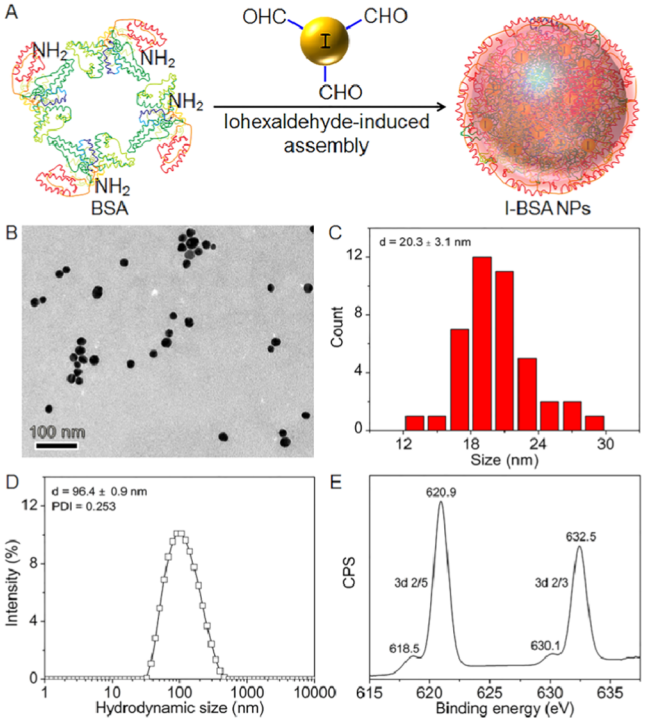

Figure 1. Preparation and characterization of I-BSA NPs. (A) Schematic diagram of the synthesis of I-BSA NPs. (B) TEM image of I-BSA NPs. (C) Size statistics of I-BSA NPs from the TEM. (D) Hydrodynamic size of I-BSA NPs dispersed in water. (E) XPS spectra of I from I-BSA NPs.

illustrates that the iohexaldehyde is used as a cross-linking agent to induce the assembly of BSA molecules via the aldimine condensation reaction. Then, the ratio of iohexaldehyde to BSA is optimized according to a uniform size and high iodine content. The result from the dynamic light scattering (DLS) and in vitro enhanced CT images shown in Figure S2 shows that the CT signal of the nanoparticles becomes stronger with the increase in the iodine content, but the size is relatively larger or even nonuniform. Therefore, the optimal molar ratio of iohexaldehyde to BSA is determined as 125:1 for preparing the I-BSA NPs. The mass percentage of iodine in each prepared nanoparticle is about 0.7% (Figure S2), which is measured by energy-dispersive X-ray spectroscopy (EDS). Transmission electron microscopy (TEM) results shown in Figure 1B indicate that the optimized I-BSA NPs have a spherical structure with an average size of 20.3 ± 3.1 nm (Figure 1C). The DLS result shown in Figure 1D confirms that the optimized I-BSA NPs have a hydrodynamic size of 96.4 nm, with a low polydispersity index of 0.253. The colloidal stability was measured by DLS over a week, and the hydrodynamic size of I-BSA NPs remains almost unchanged in water, PBS, and PBS containing 10% fetal bovine serum (FBS) (Figure S4). X-ray photoelectron spectroscopy (XPS) given in Figure 1E indicates that the peaks at 620.9 and 632.5 eV are assigned to the binding characteristic of the iodine element of iohexol. These results indicate that monodisperse and stable I-BSA NPs have been successfully prepared.

To compare the contrast performance of I-BSA NPs and iohexol, CT imaging and Hounsfield quantitative analysis over a series of the same iodine concentrations were performed. As shown in Figure 2A, the CT signal intensity of the I-BSA NPs

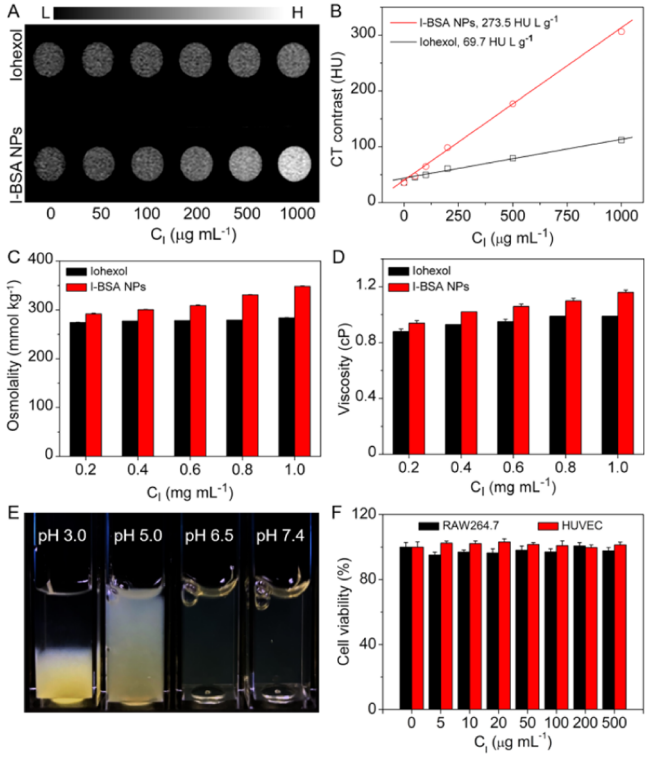

Figure 2. Properties of the prepared I-BSA NPs. (A) Concentration-dependent CT signal of I-BSA NPs and iohexol in vitro. (B) Quantitative CT contrast of I-BSA NPs and iohexol according to the concentration-dependent CT signal. (C) Osmolality and (D) viscosity of I-BSA NPs and iohexol at different concentrations. (E) Stability of the I-BSA NPs in solutions with different pH values. (F) CCK-8 assays of RAW 264.7 cells and HUVECs incubated with I-BSA NPs for 24 h at different concentrations (n = 6).

is significantly better than that of iohexol under the same iodine concentration. The linear correlation between iodine concentration and CT signal intensity reveals that the X-ray attenuation coefficient of the I-BSA NPs is 273.5 HU L g^{-1} and approximately 3.9 times higher than that recorded from the opposite iohexol (Figure 2B). The result indicates that I-BSA NPs are significantly superior to that of iohexol in enhanced CT imaging. In addition to the contrast performance, the osmolality and viscosity of the contrast agent must also be evaluated to meet the clinical requirements.[40] However, as shown in Figure 2C,D, the osmolality and viscosity of I-BSA NPs increase with the increase in concentration, similar to clinical iohexol, but the increase is slightly greater than that of iohexol. Therefore, I-BSA NPs are not suitable for intravenous administration due to potential microcirculation disorders and renal cell toxicity.[41] Since BSA has a low isoelectric point and the acidic condition of the gastric mucosa,[42,43] we reasoned that I-BSA NPs can achieve gastric deposition through oral administration. Accordingly, we investigated the stability of the I-BSA NPs in solutions with different pH values. As shown in Figure 2E, the I-BSA NPs appeared turbid at pH 5 and

https://doi.org/10.1021/acs.analchem.0c05407
Anal. Chem. XXXX, XXX, XXX−XXX

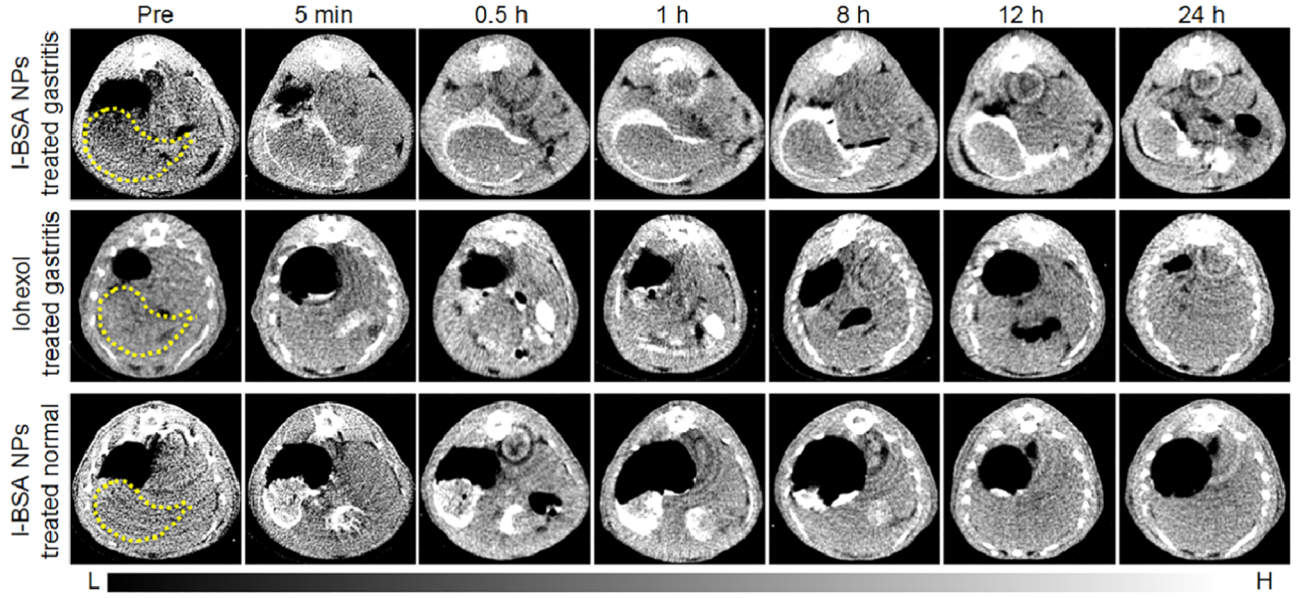

Figure 3. In vivo CT images of gastritis rats following intragastric administration with I-BSA NPs or iohexol (1 mL; 10 mg mL^{-1} I) and normal rats following intragastric administration with I-BSA NPs at different time points.

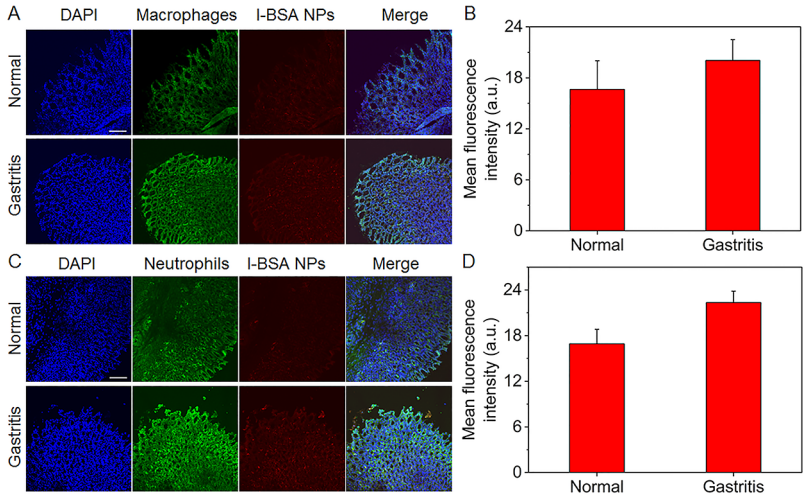

Figure 4. Immunofluorescence analysis of stomach from normal and gastritis rats treated with cypate-labeled I-BSA NPs (red; 10 μg mL^{-1}) for 24 h. Nuclei were counterstained with DAPI (blue), and images were obtained by a confocal microscope (n = 3). Scale bars = 100 μm. (A) Macrophages were stained with fluorescent-labeled anti-CD68 (green). (B) Fluorescence quantitative statistical of macrophages from CD68 by Image J software. (C) Neutrophils were stained with fluorescent-labeled anti-MPO (green). (D) Fluorescence quantitative statistical of macrophages from MPO by Image J software.

immediately precipitated at pH 3. To further explore the stability of I-BSA NPs in the simulated gastric environment, the I-BSA NPs were incubated with pepsin in the solution of different pH values. The result shown in Figure S5 indicates that pepsin can gradually digest I-BSA NPs at a low pH but reduce the potential toxicity at cellular and in vivo levels. Cytotoxicity experiments shown in Figure 2F indicate that there is no significant toxicity to macrophages (Raw 264.7) and endothelial (HUVECs) even at a high concentration of 500 μg mL^{-1} I-BSA NPs. These results illustrate that the biocompatible I-BSA NPs can be deposited on the defect mucosa under acidic conditions, which is very advantageous for the accurate diagnosis of gastritis in the early stage.

To verify the potential of I-BSA NPs for in vivo CT diagnosis, a rat model of acute gastritis was established by intragastric administration with alcohol and aspirin.[39,44] After 4 h, 1 mL of I-BSA NPs (10 mg mL^{-1} I) were injected into the stomachs of the rat model. As shown in Figure 3, the morphology of the stomach is immediately revealed by the animal CT imaging system. The result from the strong acidity and defect of the gastritic mucosa shows that the I-BSA NPs are forced to deposit on its surface, causing the signal to gradually increase. After 0.5 h of administration, the intensity of the cardia is significantly stronger than those of other parts, which may indicate that the inflammation of the cardia is more severe. The pyloric signal begins to appear at 8 h postadministration and is gradually increased. As a control, the same dose of I-BSA NPs was intragastrically injected into normal rats. The I-BSA NPs quickly settle at the bottom of the stomach without sticking to the gastric mucosa and then reach the pylorus and are excreted from the intestines. In addition, we performed enhanced CT imaging for gastritis with iohexol.

https://doi.org/10.1021/acs.analchem.0c05407
Anal. Chem. XXXX, XXX, XXX−XXX

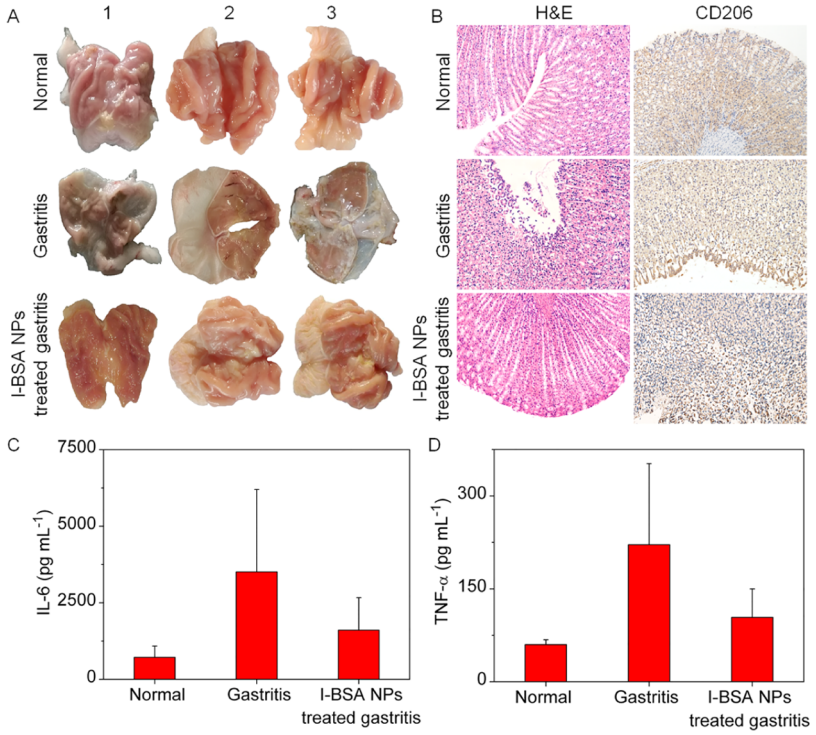

Figure 5. Repair effect and mechanism of acute gastritis with I-BSA NPs. (A) Color images (n = 3) of the stomach in normal rats, gastritis rats, and gastritis rats treated with I-BSA NPs (1 mL; 10 mg mL^{-1} I). (B) Hematoxylin and eosin (H&E) and immunohistochemistry analysis of stomach in normal rats, gastritis rats, and gastritis rats treated with I-BSA NPs. Quantification of serum IL-6 (C) and TNF-α (D) from normal rats, gastritis rats, and gastritis rats treated with I-BSA NPs by ELISA (n = 3).

After intragastric administration, it is rapidly metabolized from the intestines without leaving any signal in the stomach. These results are mainly caused by the low-molecular-weight and nonspecific intrinsic defects of a small molecule.

To further elucidate whether I-BSA NPs accumulate in inflammatory cells, the healthy and model rats were administered intragastrically with the cypate-labeled I-BSA NPs.[45] At 24 h after I-BSA NPs administration, the entire rat stomach was sectioned and immunostained. As the two pivotal roles in inflammatory responses, macrophages and neutrophils were stained with anti-CD68 and anti-MPO, as shown in Figure 4, respectively. As shown in Figure 4B,D, the mean fluorescence intensity of cypate-labeled I-BSA NPs in macrophages and neutrophils of gastritis is 20.1 and 22.4, while that in the control is 15.5 and 16.9, respectively. Therefore, we believe that the uptake of I-BSA NPs in gastritis is mainly due to the phagocytosis of inflammatory cells, including macrophages and neutrophils.

Interestingly, we find that I-BSA NPs can also effectively cure gastritis. After 24 h postadministration, all rats were anesthetized and sacrificed. The tissues of each group including the stomach were collected and washed. As shown in Figure 5A, the stomach of rats injected with I-BSA NPs returned to red, similar to that of the normal rats. While the stomach of the rats injected with iohexol showed a slight erosion given in Figure S6. Next, histopathology also validated the therapeutic function of I-BSA NPs. The longitudinal sections of the stomach were stained with hematoxylin and eosin. As shown in Figure 5B, the gastritic tissues treated with I-BSA NPs maintained an undisturbed structure with a clear layer of epithelial cells, which is similar to the gastric samples treated with PBS. While the untreated gastritis tissue shows superficial hyperemia of the mucosa, fibrous tissue hyperplasia, and inflammatory cell infiltration. The results from morphological observation and histopathological analysis indicate that I-BSA NPs have an inhibiting effect on acute gastritis.

Previous results regarding pH-responsive sedimentation of I-BSA NPs on the mucosal surface explained the specific CT imaging and repair of gastritis. However, we are most interested in exploring the mechanism of gastritis repair. To this end, we analyzed the inflammatory immune response caused by I-BSA NPs. The macrophage phenotype can be dynamically switched between proinflammatory M1 and anti-inflammatory M2 depending on their microenvironment.[46] To understand the pivotal role of macrophage phenotypes in inflammatory repair, I-BSA NP-treated gastritis and untreated controls were evaluated by immunohistochemistry at 24 h after intragastric administration. As shown in Figures 5B and S7, the presence of CD206^{+} in I-BSA NP-treated gastritis group increases 2 times compared with those of the untreated controls, representing increased quantities of M2 macrophages in I-BSA NP-treated gastritis. These results validate macrophage-dependent mechanisms of inflammatory inhibition. Accordingly, anti-inflammatory immune response to I-BSA NPs was evaluated with an enzyme-linked immunosorbent assay. We focus on the expression of cytokines related to inflammation including IL-6, and TNFα. Serum obtained from each rat was used to analyze the effect of I-BSA NPs on the host immune response. As shown in Figure 5C,D, untreated rat model results in the upregulation of IL-6 and TNFα. However, when gastritis rats are treated with I-BSA NPs, the release of these proinflammatory cytokines is significantly reduced in the gastric tissue. The results from morphological observation, histopathological analysis, and immune response indicate that I-BSA NPs have an inhibiting effect on acute gastritis.

https://doi.org/10.1021/acs.analchem.0c05407
Anal. Chem. XXXX, XXX, XXX−XXX

To evaluate the in vivo toxicity of I-BSA NPs, blood biochemical analysis and blood routine test suggest that I-BSA NPs have no significant hepatorenal toxicity, part and have no obvious effect on the indicators of blood components shown in Figure S8A. Moreover, the histopathology analysis of the tissues other than the stomach is performed, including heart, liver, spleen, lung, and kidney. Compared with those of the normal rats, no noticeable inflammation or damage is observed in these organs, as shown in Figure S8B. These results indicate that the I-BSA NPs are quite safe according to the current experimental dosage and administration method.

In conclusion, a novel iodinated BSA nanoparticle has been developed for enhanced CT imaging and repair of acute gastritis based on the gastritic microenvironment. The result from pH-responsive sedimentation shows that I-BSA NPs can adhere to the surface of the mucosa. Compared with those of the healthy rats and those with small-molecule-treated gastritis, the morphology and severity of gastritis are clearly revealed by I-BSA NPs enhanced CT imaging over a long time window. In addition, we discovered that nanoparticles have a repair effect on gastritis and investigated the repair mechanism through an inflammatory immune response. We believe that the current studies have highlighted the great potential of the novel iodinated BSA nanoparticles in gastritis theranostics.

■ ASSOCIATED CONTENT

Supporting Information

The Supporting Information is available free of charge at https://pubs.acs.org/doi/10.1021/acs.analchem.0c05407.

Reagents and materials; characterization; stability of I-BSA NPs; CCK-8 assays of I-BSA NPs; pH and pepsin-responsive study; blood analysis and histology analysis; and animal experiments (PDF)

■ AUTHOR INFORMATION

Corresponding Authors

Yangyun Wang − *State Key Laboratory of Radiation Medicine and Protection, School for Radiological and Interdisciplinary Sciences (RAD-X), Collaborative Innovation Center of Radiation Medicine of Jiangsu Higher Education Institutions, Soochow University, Suzhou 215123, China*; Email: yywang578@suda.edu.cn

Yong Wang − *State Key Laboratory of Radiation Medicine and Protection, School for Radiological and Interdisciplinary Sciences (RAD-X), Collaborative Innovation Center of Radiation Medicine of Jiangsu Higher Education Institutions, Soochow University, Suzhou 215123, China*; Email: wangyongac@gmail.com

Authors

Yanxian Wu − *State Key Laboratory of Radiation Medicine and Protection, School for Radiological and Interdisciplinary Sciences (RAD-X), Collaborative Innovation Center of Radiation Medicine of Jiangsu Higher Education Institutions, Soochow University, Suzhou 215123, China*

Jun Gu − *The Affiliated Jiangsu Shengze Hospital of Nanjing Medical University, Suzhou 215228, China*

Shaodian Zhang − *The Second Affiliated Hospital of Soochow University, Suzhou 215004, China*

Yuan Gu − *State Key Laboratory of Radiation Medicine and Protection, School for Radiological and Interdisciplinary Sciences (RAD-X), Collaborative Innovation Center of Radiation Medicine of Jiangsu Higher Education Institutions, Soochow University, Suzhou 215123, China*

Jie Ma − *State Key Laboratory of Radiation Medicine and Protection, School for Radiological and Interdisciplinary Sciences (RAD-X), Collaborative Innovation Center of Radiation Medicine of Jiangsu Higher Education Institutions, Soochow University, Suzhou 215123, China*

Leshuai W. Zhang − *State Key Laboratory of Radiation Medicine and Protection, School for Radiological and Interdisciplinary Sciences (RAD-X), Collaborative Innovation Center of Radiation Medicine of Jiangsu Higher Education Institutions, Soochow University, Suzhou 215123, China*; orcid.org/0000-0002-6919-9180

Complete contact information is available at: https://pubs.acs.org/10.1021/acs.analchem.0c05407

Author Contributions

‖Y.W. and J.G. contributed equally to the work.

Notes

The authors declare no competing financial interest.

■ ACKNOWLEDGMENTS

This work was supported by the National Natural Science Foundation of China (12075164, 21874097, and 81972964), the National Key Research Program of China (2018YFA0208800), the Suzhou Administration of Science and Technology (sys2018021), the Wujiang Science and Education Project (wwk201709), the People's Livelihood Science and Technology of Suzhou (SS201850), the Scientific Research Program for Young Talents of China National Nuclear Corporation and the Priority Academic Program Development of Jiangsu Higher Education Institutions (PAPD).

■ REFERENCES

(1) Sugano, K.; Tack, J.; Kuipers, E. J.; Graham, D. Y.; El-Omar, E. M.; Miura, S.; Haruma, K.; Asaka, M.; Uemura, N.; Malfertheiner, P. *Gut* **2015**, *64*, 1353−1367.

(2) Husebye, E. S.; Anderson, M. S.; Kampe, O. *N. Engl. J. Med.* **2018**, *378*, 1132−1141.

(3) Dellon, E. S.; Peterson, K. A.; Murray, J. A.; Falk, G. W.; Gonsalves, N.; Chehade, M.; Genta, R. M.; Leung, J.; Khoury, P.; Klion, A. D.; Hazan, S.; Vaezi, M.; Bledsoe, A. C.; Durrani, S. R.; Wang, C.; Shaw, C.; Chang, A. T.; Singh, B.; Kamboj, A. P.; Rasmussen, H. S.; Rothenberg, M. E.; Hirano, I. *N. Engl. J. Med.* **2020**, *383*, 1624−1634.

(4) Chao, C. J.; Shin, J. S.; Hsu, W. C.; Wang, P. M. *Endoscopy* **2013**, *45*, E280−E281.

(5) Howlett, M.; Chalinor, H. V.; Buzzelli, J. N.; Nhung, N.; van Driel, I. R.; Bell, K. M.; Fox, J. G.; Dimitriadis, E.; Menheniott, T. R.; Giraud, A. S.; Judd, L. M. *Gut* **2012**, *61*, 1398−1409.

(6) Eda, H.; Oshima, T.; Hirota, S.; Miwa, H. *Gut* **2020**, DOI: 10.1136/gutjnl-2020-322332.

(7) Beales, I. L. P. *Gut* **2020**, *70*, 431−432.

(8) Lalazar, G.; Doviner, V.; Ben-Chetrit, E. *N. Engl. J. Med.* **2014**, *370*, 1344−1348.

(9) Pandharipande, P. V.; Reisner, A. T.; Binder, W. D.; Zaheer, A.; Gunn, M. L.; Linnau, K. F.; Miller, C. M.; Avery, L. L.; Herring, M. S.; Tramontano, A. C.; Dowling, E. C.; Abujudeh, H. H.; Eisenberg, J. D.; Halpern, E. F.; Donelan, K.; Gazelle, G. S. *Radiology* **2016**, *278*, 812−821.

(10) Lee, B.-Y.; Ok, J.-J.; Elsayed, A. A. A.; Kim, Y.; Han, D. H. *Radiology* **2012**, *263*, 444−450.

(11) Lusic, H.; Grinstaff, M. W. *Chem. Rev.* **2013**, *113*, 1641−1666.

(12) Chen, H.; Rogalski, M. M.; Anker, J. N. *Phys. Chem. Chem. Phys.* **2012**, *14*, 13469−13486.
(13) Li, X.; Anton, N.; Zuber, G.; Vandamme, T. *Adv. Drug Delivery Rev.* **2014**, *76*, 116−133.
(14) Yeh, B. M.; FitzGerald, P. F.; Edic, P. M.; Lambert, J. W.; Colborn, R. E.; Marino, M. E.; Evans, P. M.; Roberts, J. C.; Wang, Z. J.; Wong, M. J.; Bonitatibus, P. J., Jr. *Adv. Drug Delivery Rev.* **2017**, *113*, 201−222.
(15) Liu, Y.; Ai, K.; Liu, J.; Yuan, Q.; He, Y.; Lu, L. *Angew. Chem., Int. Ed.* **2012**, *51*, 1437−1442.
(16) Ostadhossein, F.; Tripathi, I.; Benig, L.; LoBato, D.; Moghiseh, M.; Lowe, C.; Raja, A.; Butler, A.; Panta, R.; Anjomrouz, M.; Chernoglazov, A.; Pan, D. *Adv. Funct. Mater.* **2020**, *30*, No. 1904936.
(17) Oh, M. H.; Lee, N.; Kim, H.; Park, S. P.; Piao, Y.; Lee, J.; Jun, S. W.; Moon, W. K.; Choi, S. H.; Hyeon, T. *J. Am. Chem. Soc.* **2011**, *133*, 5508−5515.
(18) Wang, Y.; Xu, C.; Zhai, J.; Gao, F.; Liu, R.; Gao, L.; Zhao, Y.; Chai, Z.; Gao, X. *Anal. Chem.* **2015**, *87*, 343−345.
(19) Ai, K.; Liu, Y.; Liu, J.; Yuan, Q.; He, Y.; Lu, L. *Adv. Mater.* **2011**, *23*, 4886−4891.
(20) Son, J. S.; Park, K.; Han, M.-K.; Kang, C.; Park, S.-G.; Kim, J.-H.; Kim, W.; Kim, S.-J.; Hyeon, T. *Angew. Chem., Int. Ed.* **2011**, *50*, 1363−1366.
(21) Lee, N.; Choi, S. H.; Hyeon, T. *Adv. Mater.* **2013**, *25*, 2641−2660.
(22) Liu, Y.; Ai, K.; Lu, L. *Acc. Chem. Res.* **2012**, *45*, 1817−1827.
(23) Hyafil, F.; Cornily, J. C.; Feig, J. E.; Gordon, R.; Vucic, E.; Amirbekian, V.; Fisher, E. A.; Fuster, V.; Feldman, L. J.; Fayad, Z. A. *Nat. Med.* **2007**, *13*, 636−641.
(24) Ghaghada, K. B.; Badea, C. T.; Karumbaiah, L.; Fettig, N.; Bellamkonda, R. V.; Johnson, G. A.; Annapragada, A. *Acad. Radiol.* **2011**, *18*, 20−30.
(25) Kong, W. H.; Lee, W. J.; Cui, Z. Y.; Bae, K. H.; Park, T. G.; Kim, J. H.; Park, K.; Seo, S. W. *Biomaterials* **2007**, *28*, 5555−5561.
(26) Wang, Q.; Lv, L.; Ling, Z.; Wang, Y.; Liu, Y.; Li, L.; Liu, G.; Shen, L.; Yan, J.; Wang, Y. *Anal. Chem.* **2015**, *87*, 4299−4304.
(27) Chen, X.; Zhu, H. H.; Huang, X.; Wang, P. S.; Zhang, F. L.; Li, W.; Chen, G.; Chen, B. D. *Nanoscale* **2017**, *9*, 2219−2231.
(28) Zou, Q.; Huang, J.; Zhang, X. *Small* **2018**, *14*, No. 1803101.
(29) Yin, Q.; Yap, F. Y.; Yin, L.; Ma, L.; Zhou, Q.; Dobrucki, L. W.; Fan, T. M.; Gaba, R. C.; Cheng, J. *J. Am. Chem. Soc.* **2013**, *135*, 13620−13623.
(30) Ding, Y.; Zhang, X.; Xu, Y.; Cheng, T.; Ou, H.; Li, Z.; An, Y.; Shen, W.; Liu, Y.; Shi, L. *Polym. Chem.* **2018**, *9*, 2926−2935.
(31) Hainfeld, J. F.; Ridwan, S. M.; Stanishevskiy, Y.; Smilowitz, N. R.; Davis, J.; Smilowitz, H. M. *Sci. Rep.* **2018**, *8*, No. 13803.
(32) Zhu, Y.; Wang, X.; Chen, J.; Zhang, J.; Meng, F.; Deng, C.; Cheng, R.; Feijen, J.; Zhong, Z. *J. Controlled Release* **2016**, *244*, 229−239.
(33) Zou, Y.; Wei, Y.; Wang, G.; Meng, F.; Gao, M.; Storm, G.; Zhong, Z. *Adv. Mater.* **2017**, *29*, No. 1603997.
(34) Jung, Y.; Hwang, H. S.; Na, K. *Biomaterials* **2018**, *160*, 15−23.
(35) Gao, C.; Zhang, Y.; Zhang, Y.; Li, S.; Yang, X.; Chen, Y.; Fu, J.; Wang, Y.; Yang, X. *Polym. Chem.* **2020**, *11*, 889−899.
(36) Meng, X.; Wu, Y.; Bu, W. *Adv. Healthcare Mater.* **2020**, *10*, No. 2000912.
(37) Rugge, M.; Meggio, A.; Pravadelli, C.; Barbareschi, M.; Fassan, M.; Gentilini, M.; Zorzi, M.; De Pretis, G.; Graham, D. Y.; Genta, R. M. *Gut* **2019**, *68*, 11−17.
(38) Bjarnason, I.; Scarpignato, C.; Holmgren, E.; Olszewski, M.; Rainsford, K. D.; Lanas, A. *Gastroenterology* **2018**, *154*, 500−514.
(39) Yang, H. J.; Kim, M. J.; Kwon, D. Y.; Kang, E. S.; Kang, S.; Park, S. *J. Ethnopharmacol.* **2017**, *208*, 84−93.
(40) Park, S.-m.; Aalipour, A.; Vermesh, O.; Yu, J. H.; Gambhir, S. S. *Nat. Rev. Mater.* **2017**, *2*, No. 17014.
(41) Du, B.; Yu, M.; Zheng, J. *Nat. Rev. Mater.* **2018**, *3*, 358−374.
(42) Wang, X.; Hirmo, S.; Willén, R.; Wadström, T. *J. Med. Microbiol.* **2001**, *50*, 430−435.
(43) Shinozaki, K.; Kamada, T.; Sugiu, K.; Kusunoki, H.; Manabe, N.; Shiotani, A.; Hata, J.; Teramoto, F.; Haruma, K. *Nutr. Cancer* **2010**, *62*, 1067−1073.
(44) Kim, S. H.; Park, J. G.; Sung, G. H.; Yang, S.; Yang, W. S.; Kim, E.; Kim, J. H.; Ha, V. T.; Kim, H. G.; Yi, Y. S.; Kim, J. H.; Baek, K. S.; Sung, N. Y.; Lee, M. N.; Kim, J. H.; Cho, J. Y. *Mol. Nutr. Food Res.* **2015**, *59*, 1400−1405.
(45) Wang, Y.; Sun, Z.; Chen, Z.; Wu, Y.; Gu, Y.; Lin, S.; Wang, Y. *Anal. Chem.* **2019**, *91*, 2128−2134.
(46) DeNardo, D. G.; Ruffell, B. *Nat. Rev. Immunol.* **2019**, *19*, 369−382.

https://doi.org/10.1021/acs.analchem.0c05407
Anal. Chem. XXXX, XXX, XXX−XXX